**ORIGINAL PAPER**

# Impact of different within-canopy wind attenuation formulations on modelling sensible heat flux using TSEB

Héctor Nieto[1] · William P. Kustas[2] · Joseph G. Alfieri[2] · Feng Gao[2] · Lawrence E. Hipps[3] · Sebastian Los[3] · John H. Prueger[4] · Lynn G. McKee[2] · Martha C. Anderson[2]

## Abstract

The unique vertical canopy structure and clumped plant distribution/row structure of vineyards and orchards creates an environment that is likely to cause the wind profile inside the canopy air space to deviate from how it is typically modelled for most crops. This in turn affects the efficiency of turbulent flux exchange and energy transport as well as their partitioning between the plant canopy and soil/substrate layers. The objective of this study was to evaluate a new wind profile formulation in the canopy air space that explicitly considers the unique vertical variation in plant biomass of vineyards. The validity of the new wind profile formulation was compared to a simpler wind attenuation profile that assumes attenuation through a homogeneous canopy. We evaluated both attenuation models using measurements of wind speed in a vineyard interrow, as well as turbulent flux estimates retrieved from a two-source energy balance model, which uses land surface temperature as the key boundary condition for flux estimation. This is relevant in developing a robust remote sensing-based energy balance modelling system for accurately monitoring vineyard water use or evapotranspiration that can be applied using satellite and airborne imagery for field-to-regional scale applications. These tools are needed in intensive agricultural production regions with arid climates such as the Central Valley of California, which experiences water shortages during extended drought periods requiring an effective water management policy based on robust water use estimates for allocating water resources. Results showed that the new wind profile model improved sensible heat flux estimates (RMSE reduction from 42 to 35 W m$^{-2}$) when the vine canopy is in early growth stage resulting in a strongly clumped canopy.

## Introduction

As water resources become more limited, there is a greater need for precision agricultural management at the field/subfield-scale and hence remote sensing is becoming a powerful tool for managing irrigation, particularly for high-valued crops (Bellvert et al. 2016). Thermal remote sensing

✉ Héctor Nieto
hector.nieto@irta.cat

[1] IRTA, Institute of Agriculture and Food Research and Technology, Lleida, Spain

[2] Hydrology and Remote Sensing Lab, USDA-Agricultural Research Service, Beltsville, MD, USA

[3] Department of Plant, Soils and Climate, Utah State University, Logan, UT, USA

[4] National Laboratory for Agriculture and the Environment, USDA-Agricultural Research Service, Ames, IA, USA

allows to detect plant stress and hence, when applied within an energy balance model, allows the estimation of evapotranspiration (ET) without intensive in situ measurements related to the water balance that are usually required in energy combination equations (Ortega-Farias et al. 2007; Teixeira et al. 2007; Zhang et al. 2008). There have been numerous surface temperature-based energy balance models developed for estimating surface fluxes and ET (Kalma et al. 2008). However, many of these models used moderate resolution data that are too coarse to inform variable rate application of water or nutrients within a field (Zipper and Loheide II 2014). Furthermore, there is a growing interest in precision agriculture for partitioning evapotranspiration into crop transpiration and soil evaporation, as the latter is considered non-productive water loss from an agronomic perspective (Kool et al. 2014).

Although several remote sensing ET models have already been applied for estimating ET on vineyards, such as SEBAL (Bastiaanssen et al. 1998) or SEBS (van der Kwast et al. 2009), few of them have the capability to partition fluxes

from the vegetated canopy and the underlying soil/substrate layer. One such modelling approach is the Two Source Energy Balance-TSEB land surface scheme (Norman et al. 1995), which contains a level of complexity that has allowed successful application to many different landscapes (Kustas and Anderson 2009). As any other dual source energy balance model, TSEB requires the estimation of turbulent transport efficiency coefficients, usually related to a resistance or their reciprocal conductance (Shuttleworth and Wallace 1985; Choudhury et al. 1987; Shuttleworth and Gurney 1990; McNaughton and Van Den Hurk 1995; McInnes et al. 1996). In TSEB, $R_s$ is defined as the resistance to heat transport in the boundary layer immediately above the soil surface (s m$^{-1}$) and hence controls the evaporation process. Conversely, $R_x$ is the boundary layer resistance of the canopy of leaves (s m$^{-1}$) and controls heat and mass interchanges between the canopy and the air–canopy interspace (i.e., transpiration process). Norman et al. (1995) and Kustas and Norman (1999), based on previous studies (McNaughton and Van Den Hurk 1995; Sauer et al. 1995; Kondo and Ishida 1997), derived semi-empirical formulas for these two resistances to heat transport, which depend on the wind speed ($u_s$) at the height above the soil surface where the effect of the soil roughness is minimal ($z_{0,\text{soil}} \approx 0.01{-}0.05$ m), and the wind speed at the bulk heat source/sink $d_0 + z_{0M}$ (i.e., $u_{d_0+z_{0M}}$), respectively, for estimating $R_s$ and $R_x$. Since wind speed is attenuated when flowing through porous roughness elements such a plant canopy, adequately modelling the vertical wind profile within the canopy is needed for an accurate estimation of the resistances to heat transport, and hence for estimating evapotranspiration and its partitioning.

The TSEB modelling approach for $u_s$ and $u_{d_0+z_{0M}}$ described in Norman et al. (1995) and Kustas and Norman (1999) is based on an exponential wind attenuation proposed by Goudriaan (1977). However, this attenuation profile model was particularly designed for homogeneous and dense canopies (Goudriaan 1977). Other wind attenuation formulations are based on hyperbolic cosine mathematical relationships with the aim of simulating sparse canopies (Massman 1987) or canopies with a vertical discontinuity (Lalic et al. 2003). A previous study (Cammalleri et al. 2010) applied Goudriaan (1977), Massman (1987) and Lalic et al. (2003) profile models in TSEB over an olive orchard. From the three models tested, Cammalleri et al. (2010) found that Lalic et al. (2003) gave poor performance when comparing the estimated TSEB sensible heat flux with in situ measured fluxes, with Massman (1987) and Goudriaan (1977) yielding similar satisfactory estimates.

More recently, Massman et al. (2017) developed a new physically based wind attenuation profile that eliminates the assumptions of uniform vertical canopy structure in modelling wind attenuation throughout the canopy. Therefore this new model provides a more physically realistic method

for calculating wind speed attenuation for canopies of vertically non-uniform foliage distribution and leaf area, such as orchards and vineyards.

The objective of this study is to evaluate and compare the Massman et al. (2017) and Goudriaan (1977) wind attenuation profiles to estimate the wind speed below the canopy and the turbulent fluxes derived with TSEB in a clumped and vertically heterogeneous canopy such as a vineyard. Both Massman et al. (2017) and Goudriaan (1977) models were evaluated using in situ continuous input measurements from flux towers in two adjacent vineyards over a three year period, where different canopy vertical foliage distributions were modelled depending on phenological/management stage. In the next section we describe the implementation and inputs required for the Massman et al. (2017) wind attenuation profile model. In "Materials and methods" we describe the experimental setup while in "Results and discussion" we discuss the results. A detailed mathematical formulation in TSEB is described in the Appendix.

## Massman et al. (2017) wind profile

Compared to previously used canopy wind profiles such as Goudriaan (1977) or Massman (1987), the additional key input required in Massman et al. (2017) wind attenuation model is the relative canopy foliage distribution ha($\xi$), computed as in Eq. 1

$$\text{ha}(\xi) = \text{PAI} \frac{f_a(\xi)}{\int_0^1 f_a(\xi')\mathrm{d}\xi'} \tag{1}$$

where $\frac{f_a(\xi)}{\int_0^1 f_a(\xi')\mathrm{d}\xi'}$ is the relative canopy shape (i.e., $\sum \frac{f_a(\xi)}{\int_0^1 f_a(\xi')\mathrm{d}\xi'} = 1$, and $\xi = z/h_c$) and PAI is the plant (leaves + stems) area index. Massman et al. (2017) modelled the shape of the plant surface distribution $f_a(\xi)$ as a combination of asymmetric Gaussian curves, but $f_a(\xi)$ can also be estimated as a continuous curve obtained from canopy structure measurements or three dimensional cloud points, such as in Nieto et al. (2018).

The canopy wind speed profile is then the product of two terms: a logarithmic profile ($U_b$) that is dominant near the ground, and a hyperbolic cosine profile ($U_t$) that dominates near the top of the canopy, where the canopy foliage distribution plays a major role. Ancillary input in $U_t$ is the drag coefficient of the individual foliage elements ($C_d$), which is usually considered equal to 0.2 (Goudriaan 1977; Massman et al. 2017). Also, the Massman et al. (2017) model has the ability to consider variations of the drag coefficient due to either wind sheltering between foliage elements, or vertical variations independent of wind blocking. This effect

can usually be disregarded in most canopies (Massman et al. 2017) so was it in this study.

## Wind speed above the canopy

Most of canopy wind attenuation profiles known (Goudriaan 1977; Massman 1987; Lalic et al. 2003; Massman et al. 2017) require an estimate of the wind speed directly above the top of the canopy height ($u_c$). Assuming that wind profile above the canopy is logarithmic (Brutsaert 2005), and ignoring corrections associated to the roughness sub-layer (Raupach 1994; Massman et al. 2017), $u_c$ is estimated as (Eq. 2):

$$u_c = \frac{u_*}{\kappa'}\left[\ln\left(\frac{h_c - d_0}{z_{0M}}\right) - \Psi_m\left(\frac{h_c - d_0}{L}\right) + \Psi_m\left(\frac{z_{0M}}{L}\right)\right]$$
(2)

where $u_*$ is the friction velocity (m s$^{-1}$), $\kappa' = 0.4$ is the von Kàrman constant, $h_c$ is the canopy height (m), $d_0$ and $z_{0M}$ (m) are, respectively, the zero-plane displacement height and aerodynamic roughness length for momentum transport, and $\Psi_m\left(\frac{h_c - d_0}{L}\right) + \Psi_m\left(\frac{z_{0M}}{L}\right)$ are stability correction functions for momentum transport (Brutsaert 2005).

## Materials and methods

### Study site

Two adjacent vineyards, labeled North and South, which were planted in 2008 and 2011, respectively, at the Borden ranch near Lodi, CA (38.29°N 121.12°W), are used as part of the GRAPEX project (Kustas et al. 2018b). The management of the two vineyards, which includes the timing and amount of irrigation, pruning activities, cover crop management, and application of agrochemicals also differed from season-to-season and between the blocks due to variation in weather and climate conditions.

In both fields, the configuration of the trellising system and interrow is the same (Fig. 1). The vine trellises are 3.35 m apart and run east–west. There is an individual vine planted every 1.52 m, with the two main vine stems attached to the first cordon at a height of 1.45 m above ground level (agl). There is a second cordon at 1.9 m agl where vine shoots are managed. Typically, the vines reach a maximum height of between 2.0 m and 2.5 m agl during the growing season with the vine biomass concentrated in the upper half of the total canopy height. The typical vine canopy width is nominally 1 m mid-season. Pruning of the vines is mainly performed to remove shoots growing significantly into the interrow. Due to irrigation management practices, a grass layer in the interrow is kept in the early stages of the growing
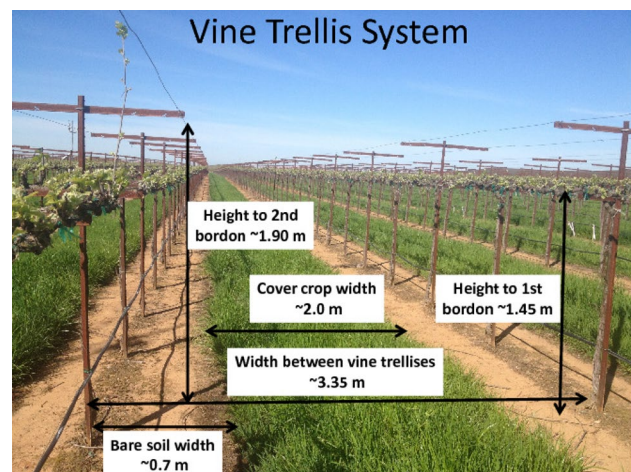


**Fig. 1** Dimensions of trellis system in both North and South vineyards

season, which is then mowed several times in spring time and allowed to go into senescence in summer.

Eddy covariance/energy balance (EC) systems were located approximately 20 m inside each vineyard at the east edge to have an adequate fetch for the prevailing winds from the west. A detailed description of the measurements and their post-processing is described by Alfieri et al. (2018b). Briefly the tower at each site is instrumented with an infrared gas analyzer (EC150, Campbell Scientific,[1] Logan, Utah) and a sonic anemometer (CSAT3, Campbell Scientific) co-located at 5 m agl to measure the concentrations of water and carbon dioxide and wind velocity, respectively. The full radiation budget was measured using a four-component net radiometer (CNR-1, Kipp and Zonen, Delft, Netherlands) mounted at 6 m agl. Air temperature and water vapor pressure at 5 m agl was measured using a Gill-shielded temperature and humidity probe (HMP45C, Vaisala, Helsinki, Finland). Subsurface measurements include the soil heat flux measured via a cross-row transect of five plates (HFT-3, Radiation Energy Balance Systems, Bellevue, Washington) buried at a depth of 8 cm. The soil heat flux was corrected for heat storage in the overlying soil layer following Oke and Cleugh (1987). Processing of turbulent data included despiking of high-frequency data (Goring and Nikora 2002), 2-D coordinate rotation of wind components (Tanner and Thurtell 1969), and Massman (2000) frequency response correction. The initial estimates of latent heat flux were corrected

---

[1] The use of trade, firm, or corporation names in this article is for the information and convenience of the reader. Such use does not constitute official endorsement or approval by the US Department of Agriculture or the Agricultural Research Service of any product or service to the exclusion of others that may be suitable.

| Site | IOP | Start date | End date |
|------|-----|-----------|----------|
| N | 2 | 1 June 2015 | 3 June 2015 |
| | 4 | 10 August 2015 | 13 August 2015 |
| S | 2 | 31 May 2015 | 3 June 2015 |
| | 3 | 10 July 2015 | 13 July 2015 |
| | 4 | 10 August 2015 | 13 August 2015 |

*IOP* intensive observation period

for density effects following Webb et al. (1980), whereas sensible heat flux estimates were corrected for buoyancy effects (Foken 2008).

With the purpose of estimating fluxes from the soil/grass layer system, and to evaluate the turbulence intermittency between the above and below vine canopy, one additional eddy covariance system was placed in each vineyard in the interrow space at a height of 1.45 m during Intensive Observation Periods in 2015. Table 1 shows the dates for each site when wind speed below the canopy is available. A more detailed description of all experiments and measurements taken during the GRAPEX experiment is described in Kustas et al. (2018b).

## Model evaluation

Both Massman et al. (2017) and Goudriaan (1977) wind attenuation profiles were evaluated to assess their performance in estimating below-canopy wind attenuation speed in the interrow space at 1.45 m (namely $u_{z,\text{ref}}$), using input data from atmospheric measurements above the crop together with estimates of canopy structure, and validated using the wind speed from the deployed EC in the interrow during IOPs in 2015. Also, we evaluated the capability of both attenuation profiles to estimate above-canopy bulk sensible heat flux $H$ in TSEB. Both variables were evaluated in terms of percentage of variance explained by the model ($R^2$), as well as error measurement metrics such as mean bias, Mean Absolute Error MAE, Root Mean Square Error RMSE, and its decomposition between systematic and unsystematic RMSE (Willmott 1981). Significant differences in errors between both models were tested using Student's t-test, establishing the null hypothesis that the mean error, mean absolute error, or mean squared error are equal between Massman et al. (2017) and Goudriaan (1977) models.

To run both attenuation profile models as well as TSEB, several ancillary canopy properties (i.e., Leaf Area Index, canopy height, foliage distribution density) were estimated on a daily basis using combined information from Landsat and MODIS satellites.

## Estimation of daily canopy properties

Estimates of bulk LAI (i.e., leaf area of grapevines and grass) were obtained by fusing MODIS LAI (MCD15A3H) product and Landsat surface reflectance using the reference-based approach (Gao et al. 2012, 2014). The homogeneous and high-quality LAI retrievals from the MODIS LAI product were extracted to train Landsat surface reflectance aggregated at the MODIS spatial resolution. The trained regression trees were then applied to original 30 m Landsat surface reflectance to produce Landsat LAI. Since the study sites are located in an area that is overlapped by two Landsat paths and are normally cloud free, more than 60 clear Landsat observations were acquired for each year. Daily LAI at 30 m Landsat resolution were generated using the Savitzky–Golay moving window filter approach which smooths and fills the temporal gaps (Sun et al. 2017).

Canopy width $w_c$, canopy height $h_c$, the height of the bottom of the canopy $h_b$ and the green fraction $f_g$ were estimated from the daily LAI using empirical curves fit with measured in situ values during four Intensive Observation Periods in 2015 (Fig. 2). The empirical fits were constrained by the following boundary conditions based on Fig. 1:

- canopy height should tend to the height of the vine trellis when LAI tends to zero, as this is where the branches with sprouts are located:

$$\lim_{\text{LAI}\to 0} h_c = 1.45\,\text{m}$$

- canopy width should tend to the width of the vine trellis when LAI tends to zero, as the branches with sprouts follows a "T" pattern:

$$\lim_{\text{LAI}\to 0} w_c = 0.60\,\text{m}$$

- the height of the bottom of the canopy tends to $h_c$ when LAI tends to zero. In other words, the ratio of bottom-to-top of the canopy $h_b/h_c$ tends to 1 when LAI tends to zero.

$$\lim_{\text{LAI}\to 0} \frac{h_b}{h_c} = 1$$

- the green fraction is held constant to 1 during the growing season until observed senescence from daily phenocam photos near flux towers (typically mid September), afterwards $f_g$ linearly decreases with LAI, tending to 0 when LAI is zero.

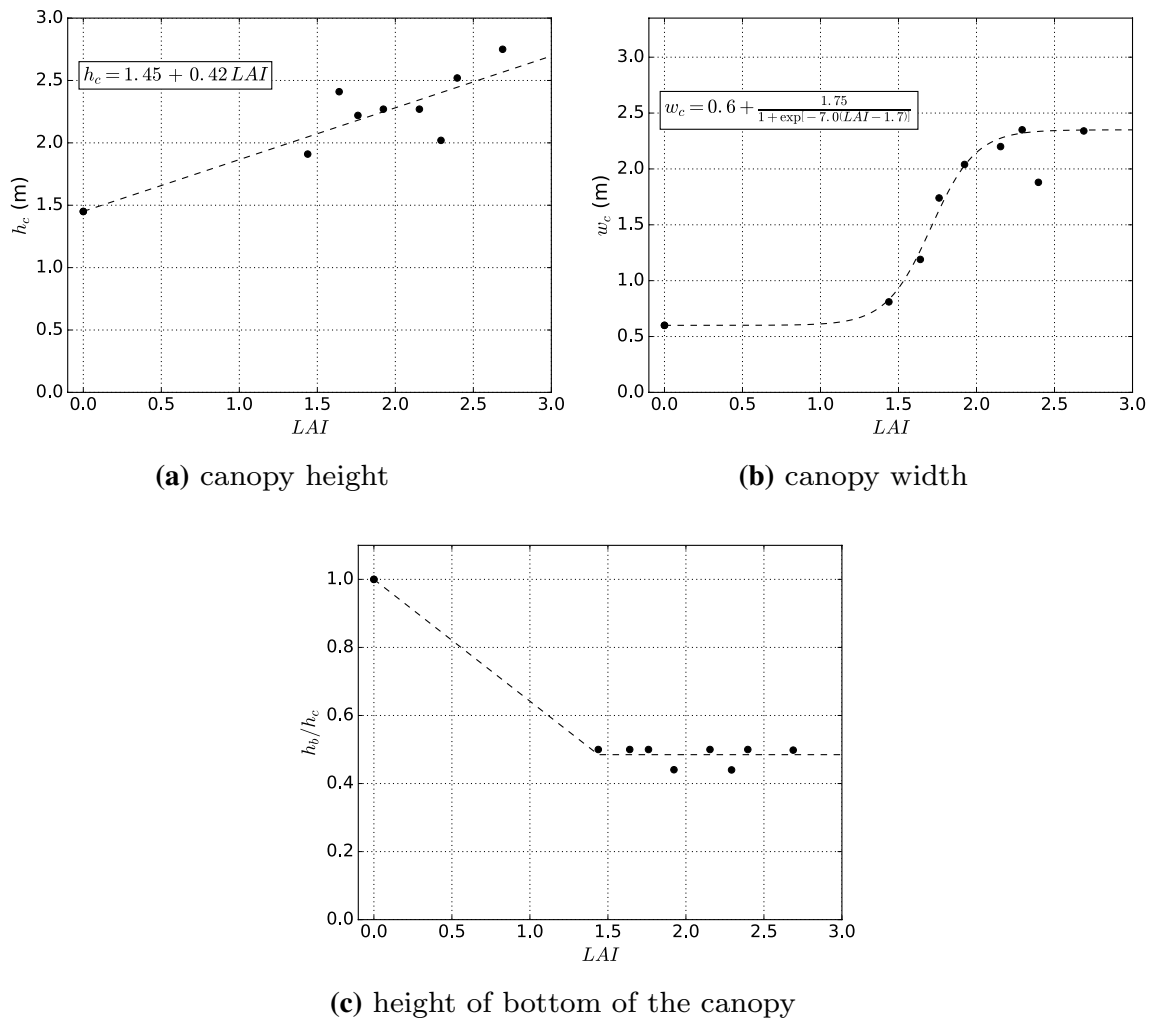$$\lim_{\text{LAI}\to 0} f_g = 0; \quad \text{when DOY} > 250.$$

**(a)** canopy height

**(b)** canopy width

**(c)** height of bottom of the canopy

**Fig. 2** Empirical models relating canopy height $h_c$, canopy width $w_c$ and the bottom of the canopy $h_b$ with the fused STARFM LAI. Solid dots represent in situ measured values

Figure 3 shows the timeseries of LAI and green fraction $f_g$ in both vineyards spanning the whole study period (2014–2016). Since the Landsat LAI product represents 30 m effective LAI values, the decreases in LAI in springtime are due to grass mowing management. Neither LAI or $f_g$ reach to zero since at the time of grapevine senescence and leaf-off in autumn, there is a regrowth of the grass layer in the interrow.

The relative foliage density profiles required in Massman et al. (2017) wind attenuation profile are derived after visual inspection of daily phenocam photos (Fig. 4). At our study site, there is a canopy overstory comprised of vertically non homogeneous biomass/leaf area, as grapevines are usually clumped due to the trellis system and pruning, and an understory at ground level having a dense layer of cover crop, which eventually is mowed and finally becomes stubble later during the growing season (early June). Therefore, we assumed our canopy foliage distribution changes

with seasons/phenological stages. Before grapevine bud-break the only photosynthetic element is the grass layer in the interrow, but the trellis system and grapevine branches are still present and hence they provide additional roughness and wind attenuation. After bud-break (usually around mid March) there is a rapid increase of foliage biomass at the grapevine overstory and hence we assume the vineyard foliage distribution is represented as a bimodal asymmetric Gaussian function, with a higher relative foliage distribution at the grapevine canopy, until grass is mowed (typically in the beginning of May). Later on, when no standing grass is present, only the grapevine foliage contributes to the aboveground biomass, which due to the weight of fully developed branches and fruits the height at maximum foliage density tends to get closer to the ground. Finally, after leaf-off (at the end of November) there is still some attenuation due to the leafless vine shoots, and the regrowth of the cover crop.
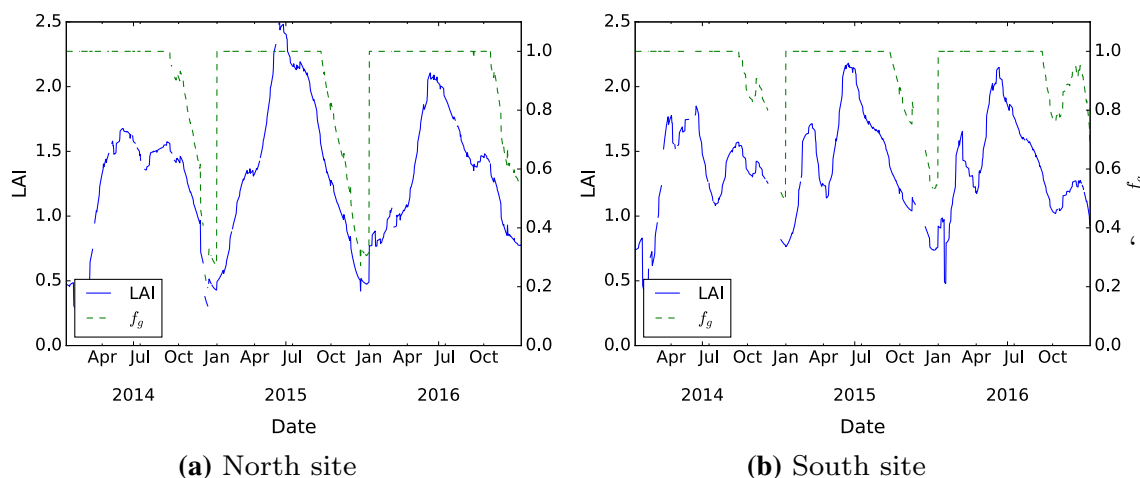
**(a)** North site

**(b)** South site

**Fig. 3** Timeseries of daily estimates for LAI and green fraction at North (left) and South (right) vineyard

## TSEB evaluation with in situ surface temperature

To evaluate the effects of the modifications in TSEB model mentioned in the previous section, we used in situ data measured at the two EC towers installed over the study area. We used the 2014–2016 year periods using 15 min averaged values during daytime (i.e., solar irradiance $S^\downarrow > 100\,\mathrm{W\,m^{-2}}$). Surface composite temperate $T_\mathrm{rad}$ was estimated from the 4-component net radiometer, Eq. 3:

$$T_\mathrm{rad} = \left( \frac{L^\uparrow - (1 - \epsilon_\mathrm{surf})L^\downarrow}{\sigma \epsilon_\mathrm{surf}} \right)^{1/4} \tag{3}$$

where $L^\uparrow$ and $L^\downarrow$ are the upwelling and downwelling measured longwave radiance, $\sigma$ is the Stefan–Boltzmann constant, and $\epsilon_\mathrm{surf} = 0.99 f_\mathrm{C} + 0.94(1 - f_\mathrm{C})$ is the surface emissivity, assuming leaf and bare soil emissivity values of 0.99 and 0.94, respectively (Sobrino et al. 2005).

Additional inputs from the EC system were downwelling shortwave $S^\downarrow$ irradiance, wind speed and direction, air temperature and humidity, and atmospheric pressure, all of them measured at 5 m above the ground. Furthermore, to reduce the uncertainties in modelling the flux partitioning associated to errors in the estimation of soil heat flux, we forced TSEB to use the estimated $G$ by the EC system instead of making an estimate based on $R_{n,S}$ (Choudhury et al. 1987; Santanello Jr and Friedl 2003). Details on TSEB modelling are addressed in Appendix, and in Norman et al. (1995), Kustas and Norman (1999) and Kustas et al. (2016). A version of the TSEB model is available online at https://github.com/hectornieto/pyTSEB.

*Aerodynamic resistances parameterization* Kustas et al. (2016) showed that in case of sparse and heavily clumped vegetation and/or when the soil surface is very rough, the values

for the $C'$, $b$ and $c$ parameters in the Kustas and Norman (1999) soil ($R_\mathrm{s}$, Eq. 7b) and canopy boundary layer ($R_x$, Eq. 7c) resistances for heat transport might deviate from the default values proposed in Kustas and Norman (1999) and Norman et al. (1995). In our case we follow this rationale assuming that the soil is rougher than usual due to the presence of a grass stubble layer. Therefore, we used in the estimation $R_\mathrm{s}$ the value $c = 0.0038\,\mathrm{m\,s^{-1}\,K^{-1/3}}$ for a rough soil surface suggested in Kondo and Ishida (1997) and used successfully in Kustas et al. (2016). The estimation of aerodynamic roughness length and zero-plane displacement height considered the effects of wind direction relative to row orientation, as observed and modelled by Alfieri et al. (2018a), with larger roughness values at the across-row than the down-row winds.

*Net radiation partitioning for row crops* We developed a simplified method to derive the clumping index in row crops such as vineyards (Parry et al. 2018). The new clumping index is based on the ideas of the geometric model by Colaizzi et al. (2012), but instead of considering the crops as elliptical hedgerows, we assumed a rectangular canopy shape, which simplifies the trigonometric calculations. The clumping index is defined as the factor that modifies the LAI of a real canopy ($F$) in a fictitious homogeneous canopy with $\mathrm{LAI_{eff}} = \Omega F$ such as its gap fraction is the same as the gap fraction of the actual canopy ($G(\theta, \phi)$). This effective LAI is then used as input in the Campbell and Norman (1998) canopy radiative transfer model to estimate soil and canopy net radiation.

## Results and discussion

### Wind attenuation profile evaluation

Figure 5 is a the scatterplot between measured and modelled wind speed at 1.45 m ($u_{z,\mathrm{ref}}$) using both profiles compared to

**Fig. 4** Representative pheno-cam snapshots (left panels) and modelled relative foliage distribution function (right panels) for the different seasons/stages considered in this study: bud-break, spring, summer and leaf-off
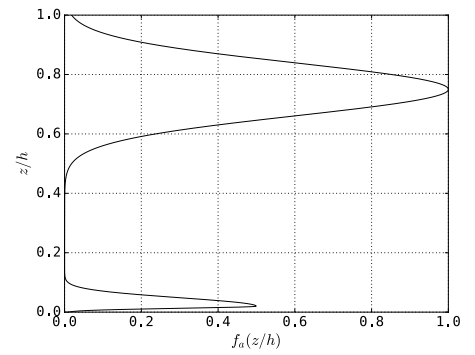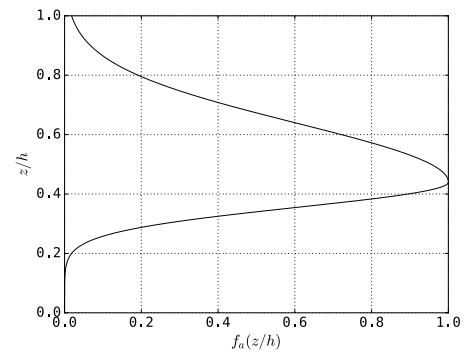


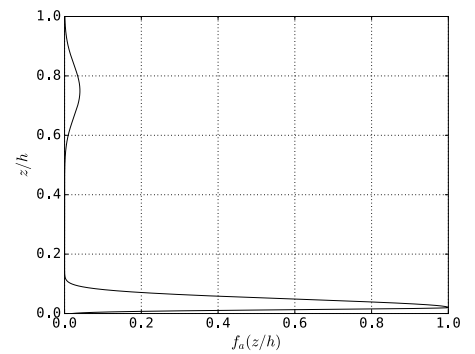**(a)** Bud-break
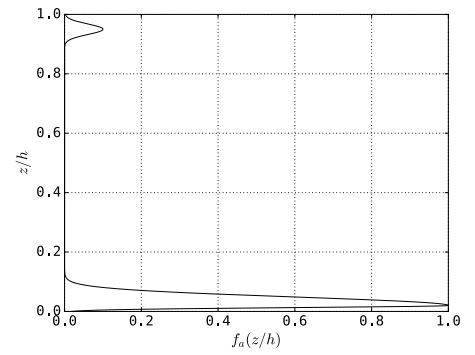


**(b)** Bud-break



**(c)** Spring



**(d)** Spring



**(e)** Summer



**(f)** Summer



**(g)** Leaf-off



**(h)** Leaf-off

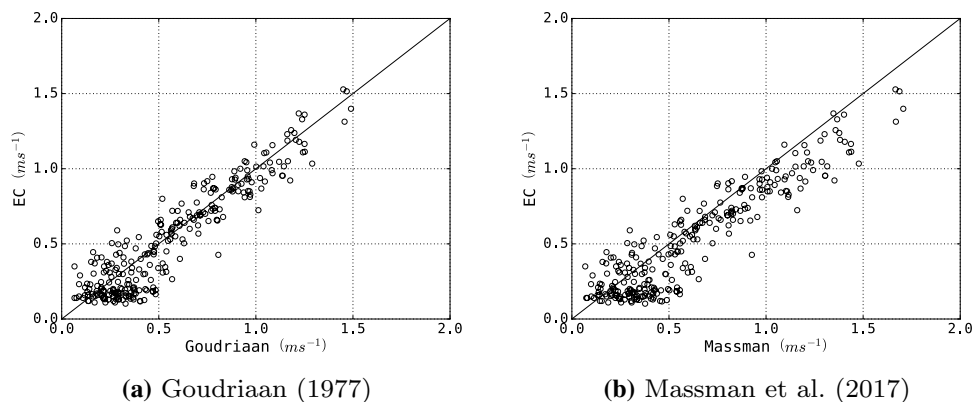**(a)** Goudriaan (1977)



**(b)** Massman et al. (2017)

**Table 2** Error assessment of wind speed at 1.45 m ($u_{z,\text{ref}}$, m s$^{-1}$) using Goudriaan (1977) and Massman et al. (2017) wind attenuation profiles

| Site | Model | Bias | MAE | RMSE | RMSE$_u$ | RMSE$_s$ | $R^2$ |
|------|-------|------|-----|------|----------|----------|-------|
| N | Goudriaan (1977) | 0.01 | 0.08 | 0.11 | 0.10 | 0.03 | 0.86 |
|   | Massman et al. (2017) | 0.05** | 0.10* | 0.12 | 0.11 | 0.05 | 0.86 |
| S | Goudriaan (1977) | 0.05 | 0.12 | 0.15 | 0.13 | 0.07 | 0.87 |
|   | Massman et al. (2017) | 0.13** | 0.17** | 0.21** | 0.16 | 0.13 | 0.86 |
| Both | Goudriaan (1977) | 0.03 | 0.10 | 0.13 | 0.12 | 0.05 | 0.87 |
|   | Massman et al. (2017) | 0.10** | 0.14** | 0.17** | 0.15 | 0.10 | 0.85 |

Error metrics significantly different between Massman et al. (2017) and Goudriaan (1977) are flagged with an asterisk (*) when Student's *t* test showed that averages were significantly different at 95% confidence, and with a double asterisk (**) at 99% confidence

the in situ horizontal wind speed from the sonic anemometer placed at 1.45 m agl. The scatterplot shows that $u_{z,\text{ref}}$ modelled with Goudriaan (1977) fits closer to the 1:1 line compared to Massman et al. (2017). This surprising result is numerically shown in Table 2, which lists the error statistics for IOPs in 2015 when the below-canopy EC system was operating. Goudriaan (1977) has a higher coefficient of determination (i.e., higher $R^2$), it yields significantly lower errors, with bias closer to 0 than Massman et al. (2017) and lower Mean Absolute Error and Root Mean Square Error.

Table 2 indicates a slight-to-moderate better performance with the original Goudriaan (1977) wind speed at 1.45 m agl, a height at which the attenuation due to the grapevine is significant. In fact, a comparison of the wind attenuation profiles using Massman et al. (2017) and Goudriaan (1977) is shown in Figs. 6 and 7 illustrate the wind attenuation profiles of Goudriaan and Massman for a canopy with total LAI = 2 and a canopy height of 2 m. Figure 6 represents the four different attenuation profiles corresponding to the foliage densities used in this study and previously illustrated in Fig. 4. Comparison between the two figures demonstrates more clearly the effect of non-uniform vertical profile, particularly near the soil surface. Furthermore, Massman et al. (2017) attenuation profiles also significantly differ between growth stages, with very little attenuation at the vine canopy/trellis system before bud-break and after leaf-off. Since in

the summer stage the grapevine canopy is well developed, spreading towards both the interrow and the ground (see Fig. 4e, f), its attenuation becomes more uniform compared to earlier in the growing season (Fig. 6b vs. Fig. 6c). Finally, it is worth noting that Goudriaan (1977) attenuation profile (Fig. 7) seems to provide unrealistic values near the soil, as it has been observed that wind speed near the soil should tend to zero (Heilman et al. 1994, Fig. 5).

It is worth noting that the effect of wind direction on wind attenuation, which was already observed in vineyards by Heilman et al. (1994), is implicitly considered on the roughness dependence on the wind direction relative to the row orientation (Alfieri et al. 2018a). Figure 8 shows a typical wind attenuation profile when wind direction is parallel to the rows (i.e., down-row wind, dashed red line) and perpendicular to the rows (i.e., cross-row wind, dotted blue line). This figure shows a stronger attenuation, both above and below the canopy, when wind blows in the cross-row direction, and is an effect that is in agreement with the observations from Heilman et al. (1994, Fig. 4)

## Evaluation in TSEB

The TSEB sensible heat flux estimates (*H*) using Massman and Goudriaan wind profiles are compared to measured 15 min flux data for both sites between years 2014 and

**Fig. 6** Massman et al. (2017) wind profile attenuation $(u(z)/u(h_c))$ for a leaf area index, LAI = 2, and canopy height $h_c$ = 2 m, corresponding to the relative foliage distributions shown in Fig. 4. Red dots indicate relevant heights for this study ($z_{ref}$, $z_{d_0+z_{0M}}$ and $z_{0,soil}$). (Color figure online)
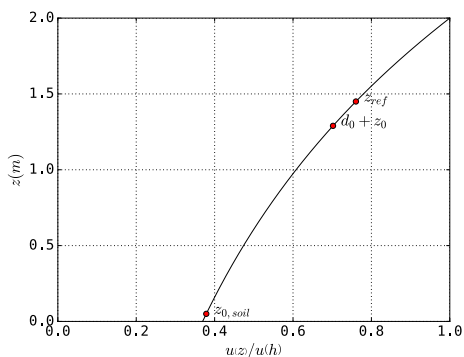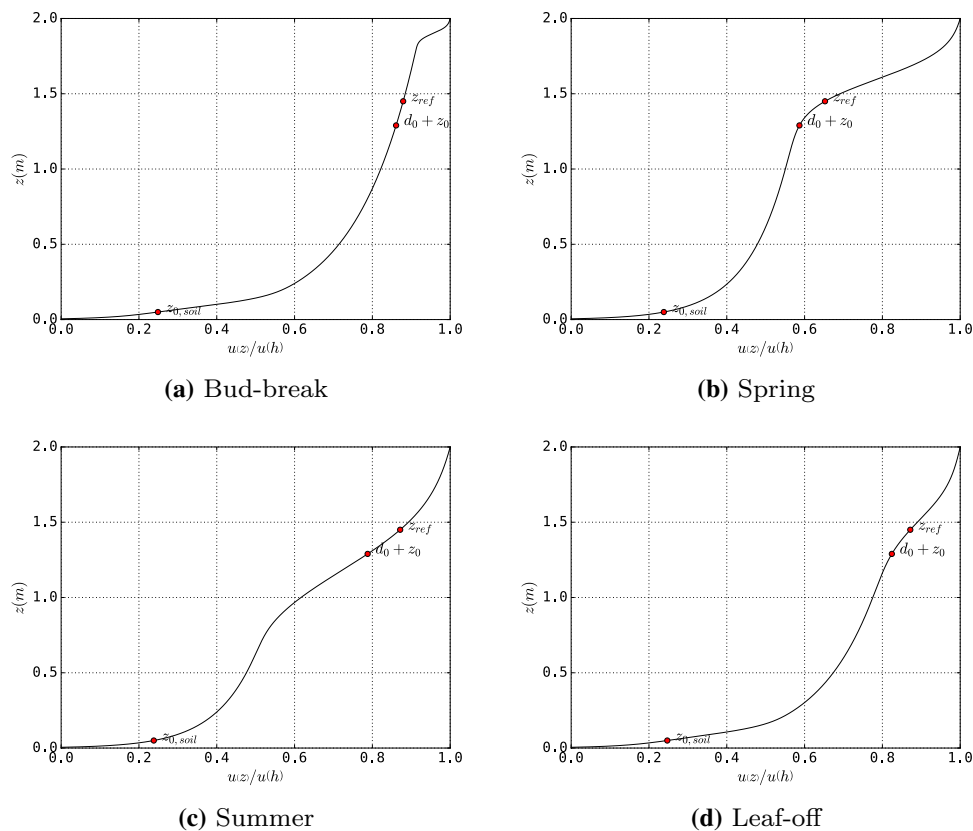
**(a)** Bud-break

**(b)** Spring

**(c)** Summer

**(d)** Leaf-off

**Fig. 7** Goudriaan (1977) wind profile attenuation $(u(z)/u(h_c))$ for a leaf area index, LAI = 2, canopy height $h_c$ = 2 m and leaf width $l_w$ = 0.1 m. Red dots indicate relevant heights for this study ($z_{ref}$, $z_{d_0+z_{0M}}$ and $z_{0,soil}$). (Color figure online)

**Fig. 8** Standard wind profiles $u$ estimated for both the down-row direction (dotted red line) and cross-row direction (dashed blue line). Profiles assume neutral conditions, 3.5 m s$^{-1}$ wind speed at 5 m above ground level, and a standard vineyard canopy with LAI = 2 and other canopy parameters retrieved based on curves of Fig. 2. The horizontal line represents the canopy height, below which the Massman et al. (2017) attenuation profile was applied. (Color figure online)

2016. The model inter-comparison is evaluated for $H$ only since errors in $R_n$ and $G$ will add noise and $H$ is directly computed by TSEB while $\lambda E$ is solved as a residual. Table 3 lists the sensible heat flux $H$ error statistics corresponding to the TSEB runs using either Goudriaan (1977) or Massman et al. (2017) models. Error metrics include the 3 years studied (2014–2016) for the two sites. Despite of the fact that Table 2 showed a better accuracy in wind speed at 1.45 m for Goudriaan (1977) model, comparison between attenuation
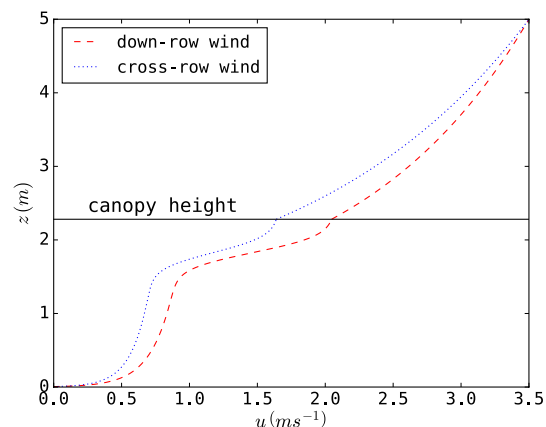
profiles implemented in TSEB did not show any significant difference, except Goudriaan (1977) attenuation showing a mean bias closer to zero, and Massman et al. (2017) having a larger $R^2$, but both models yielding similar RMSE of 42–43 W m$^{-2}$ and 41–42 W m$^{-2}$ for the north (N) and south

**Table 3** Error statistics for estimates of $H$ running TSEB with Goudriaan (1977) and Massman et al. (2017) attenuation profiles

| Model | Site | Bias | MAE | RMSE | RMSE$_u$ | RMSE$_s$ | $R^2$ |
|---|---|---|---|---|---|---|---|
| Goudriaan (1977) | N | − 13 | 30 | 42 | 32 | 27 | 0.71 |
|  | S | − 8 | 29 | 41 | 36 | 21 | 0.72 |
|  | Both | − 10 | 30 | 42 | 34 | 24 | 0.71 |
| Massman et al. (2017) | N | − 17** | 31** | 43 | 29 | 32 | 0.73 |
|  | S | − 12** | 30 | 42 | 33 | 26 | 0.73 |
|  | Both | − 15** | 30** | 43 | 31 | 29 | 0.73 |

Error measurements expressed in W m$^{-2}$. Error metrics significantly different between Massman et al. (2017) and Goudriaan (1977) are flagged with an asterisk (*) when Student's $t$ test showed that averages were significantly different at 95% confidence, and with a double asterisk (**) at 99% confidence

**Table 4** Error statistics for estimates of H at local noon for the period 2014–2016 running TSEB with Goudriaan (1977) and Massman et al. (2017) attenuation profiles

| Model | Bias | MAE | RMSE | RMSE$_u$ | RMSE$_s$ | $R^2$ |
|---|---|---|---|---|---|---|
| Goudriaan (1977) | − 16 | 41 | 54 | 45 | 31 | 0.49 |
| Massman et al. (2017) | − 22** | 40 | 54 | 40 | 37 | 0.50 |

Error measurements expressed in W m$^{-2}$. Error metrics significantly different between Massman et al. (2017) and Goudriaan (1977) are flagged with an asterisk (*) when Student's $t$ test showed that averages were significantly different at 95% confidence, and with a double asterisk (**) at 99% confidence

(S) sites, respectively. Conversely, TSEB errors seem to be slightly larger for the N site, with larger bias, MAE, RMSE and $R^2$ than in the S site. Moreover these errors are fairly consistent between the years (results not shown), which indicates some degree of robustness in TSEB modelling.

Results listed in Table 3 give the performance for all in situ observations measured during daytime (i.e., $S_{dn} > 100\,\mathrm{W\,m^{-2}}$). To allow a more straightforward comparison against model performance from other studies that were using satellite or airborne data, Table 4 shows similar statistics for both wind profiles at local noon (12 PM), time near the acquisition time of most of sun-synchronous satellites (see Kustas et al. (2018a), Nieto et al. (2018) or Knipper et al. (2018) in this issue for detailed discussions on errors in TSEB and comparison with published literature). Again, wind attenuation schemes yield the same error statistics with 41 W m$^{-2}$ MAE, 55 W m$^{-2}$ RMSE, and a determination coefficient of 0.50. Only mean bias showed significant differences between attenuation profiles, with Goudriaan (1977) model showing lower bias (−16 W m$^{-2}$) compared to Massman et al. (2017) profile (−22 W m$^{-2}$).

Nevertheless, a more detailed seasonal analysis of error assessment for both attenuation models was performed where the whole timeseries for both Goudriaan (1977) and Massman et al. (2017) TSEB implementations are separated by the different growth stages described in "Estimation of daily canopy properties". Table 5 lists the errors, for what we defined "spring" or bud-break through flowering stage (between 15 March and 1 May). Results for the other stages are not shown in Table 5 as no significant differences were found between models.

Results in Table 5 indicate that at this stage, when grapevine canopy is more vertically clumped and there is still a photosynthetic grass layer (Fig. 4c, d), most of the error statistics for modelled sensible heat flux are significantly (based on the $t$ test statistic) reduced with Massman et al. (2017) wind profile. This fact is evident in the S site, with a reduction of 84% in bias, 22% in MAE, and 26% in RMSE. These results confirms the observations by Cammalleri et al. (2010), who stated that within-canopy wind profile modelling has a larger impact in TSEB estimated $H$ for sparse and clumped vegetation. Actually, the wind profile modelled for the spring or early vine growth stage in Fig. 6b seems quite distinct compared to Goudriaan (1977) exponential attenuation (Fig. 7), causing significantly different wind speeds at both canopy sink/source height (i.e., at $d_0 + z_{0M}$) and near the soil surface ($z_{0,soil}$). This issue is confirmed in Fig. 9, where modelled wind speed at these two relevant heights (Fig. 9a, b) and their corresponding estimated resistances to heat transport (Fig. 9c, d) are quite different using Goudriaan (1977) versus Massman et al. (2017).

Modelled wind speed near the soil surface consistently yields ca. two times lower values using Massman et al. (2017) (Fig. 9a), as in this model the wind speed attenuates asymptotically to zero near the soil surface (Fig. 6). This is reflected in the estimation of the resistance to heat transport near the soil layer, with overall larger $R_s$ values in Massman et al. (2017) (Fig. 9c), but those differences are not as strong

**Table 5** Springtime error statistics for estimates of $H$ running TSEB with Goudriaan (1977) and Massman et al. (2017) attenuation profiles

| Site | Model | Bias | MAE | RMSE | $RMSE_u$ | $RMSE_s$ | $R^2$ |
|------|-------|------|-----|------|----------|----------|-------|
| N | Goudriaan (1977) | 1 | 25 | 36 | 36 | 5 | 0.77 |
| | Massman et al. (2017) | − 15** | 25 | 36 | 29 | 22 | 0.79 |
| S | Goudriaan (1977) | 19 | 32 | 47 | 43 | 20 | 0.75 |
| | Massman et al. (2017) | 3** | 25** | 35** | 34 | 6 | 0.77 |
| Both | Goudriaan (1977) | 10 | 28 | 42 | 41 | 10 | 0.74 |
| | Massman et al. (2017) | − 6** | 25** | 35** | 33 | 12 | 0.76 |

Error measurements expressed in W m$^{-2}$. Error metrics significantly different between Massman et al. (2017) and Goudriaan (1977) are flagged with an asterisk (*) when Student's $t$ test showed that averages were significantly different at 95% confidence, and with a double asterisk (**) at 99% confidence

**Fig. 9** Scatterplots between modelled wind speed (top) and resistances (bottom) using Massman et al. (2017) and Goudriaan (1977) profile models



**(a)** $u_s$

**(b)** $u_{d_0 + z_{0M}}$

**(c)** $R_s$

**(d)** $R_x$
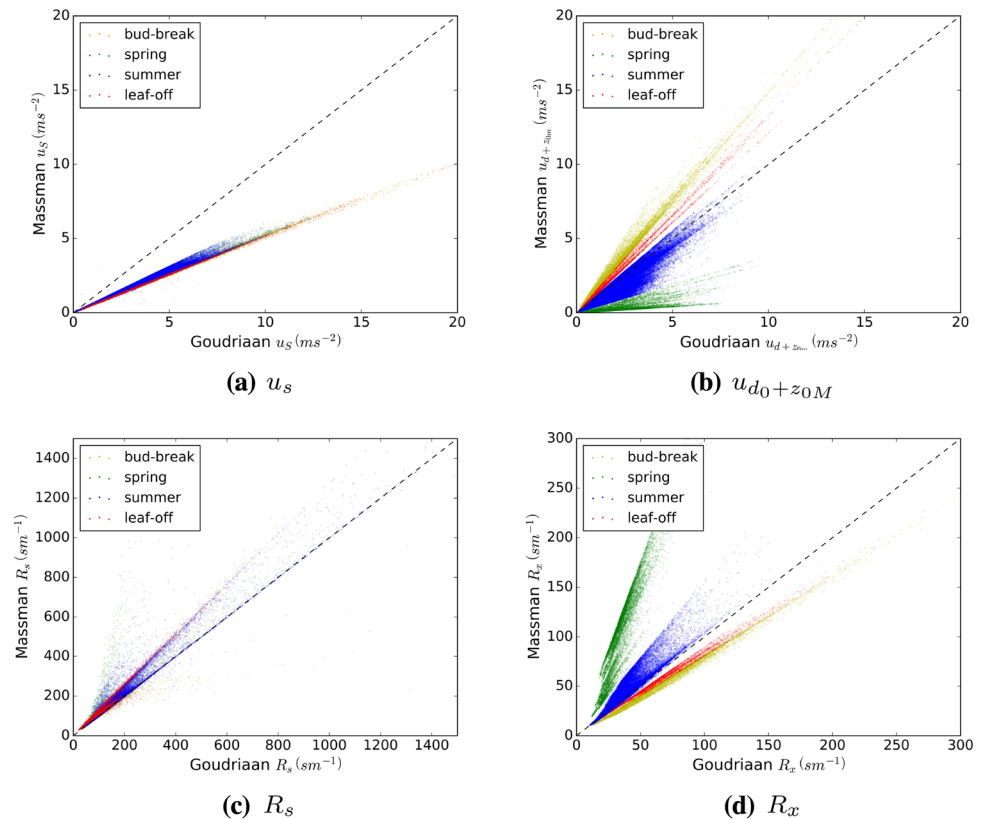
as with $u_s$ (Fig. 9c vs. Fig. 9a). This is due to the fact that $R_s$ in TSEB not only depends on wind speed but also on the buoyancy near the soil, expressed as the temperature gradient between the soil surface and the overlying air (see A, Eq. 7b and Kustas and Norman 1999). Besides, small differences were found in modelled $u_s$ between stages, since Massman et al. (2017) models the wind attenuation near the soil surface as a logarithmic function where canopy foliage plays a lesser role (Massman et al. 2017). On the other hand, significant differences are found in the estimation of wind speed at $d_0 + z_{0M}$ (Fig. 9b) and its related resistance to heat transport at the canopy boundary layer $R_x$. In spring, Massman et al. (2017) yields smaller values at $u_{d_0 + z_{0M}}$ than Goudriaan (1977), whereas in summer similar values

are produced in both models and larger speeds are usually modelled before grapevine bud-break and after leaf-off. This effect is directly affecting the estimation of $R_x$ (Fig. 9d), with significantly different values in the modelled $R_x$ between Goudriaan (1977) and Massman et al. (2017) during spring. Wind attenuation in the interrow was validated only during the IOPs showed in Table 1, which correspond mostly to dates during summer (after mowing of cover crop). Therefore we hypothesize that a larger improvement in the wind attenuation assessment would be observed in Table 2 and Fig. 5 if below-canopy wind speed measurements were available earlier in the season. Likewise, the "spring" stage is a relatively short period spanning from mid-March to early May or 1 1/2 months and hence its contribution to the overall
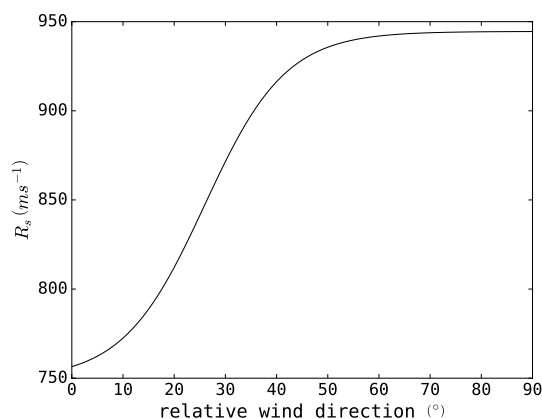
**Fig. 10** Standard aerodynamic soil resistance $R_s$ estimated at different wind directions relative to the row orientation using Massman et al. (2017) wind attenuation model. $R_s$ was computed using Kustas and Norman (1999) equation for neutral conditions, 3.5 m s$^{-1}$ wind speed at 5 m above ground level, and a standard vineyard canopy with LAI = 2 and other canopy parameters retrieved based on curves of Fig. 2



**Fig. 11** Scatterplots and timeseries between modelled Massman et al. (2017) and Goudriaan (1977) latent heat flux partitioning $\lambda E_C / \lambda E$

performance in TSEB is relatively small, as seen in Tables 3 and 4. However this period is when decisions about water status in the root zone and initiation of irrigation is being made, so it is crucial to have an accurate accounting of water use by the vines and cover crop.

Based on the results in Fig. 8, the effect of wind direction on soil aerodynamic resistance is illustrated in Fig. 10. As expected, aerodynamic resistance near the soil surface is lower when wind is blowing parallel to the rows, as lower wind attenuation occurs (Fig. 8). This effect is also observed on the average conductance values (the reciprocal of resistances) measured at the soil surface by McInnes et al. (1996, Fig. 3). Both modelled (this study) and measured (McInnes et al. 1996) showed a sinusoidal increase (decrease) of soil resistance (conductance) when wind direction changes from parallel (0°) to perpendicular (90°) to the rows.

Finally, the fact that significant differences were found in $R_s$ and primarily in $R_x$ during spring are also reflected in latent heat flux partitioning between canopy transpiration and soil evaporation (Fig. 11). Massman et al. (2017) yields slightly lower values in $\lambda E_C / \lambda E$ (Fig. 11). These lower values in spring appear to be consistent with estimates coming from using the correlation-based flux partitioning method with the high-frequency eddy covariance data (Scanlon and Sahu 2008; Scanlon and Kustas 2010, 2012) summarized in Kustas et al. (2018a).

## Discussion on irrigation management

Many studies on irrigation have quantified crop water needs using tabulated or empirically retrieved crop coefficient (Girona et al. 2006; Romero et al. 2014; Intrigliolo et al.
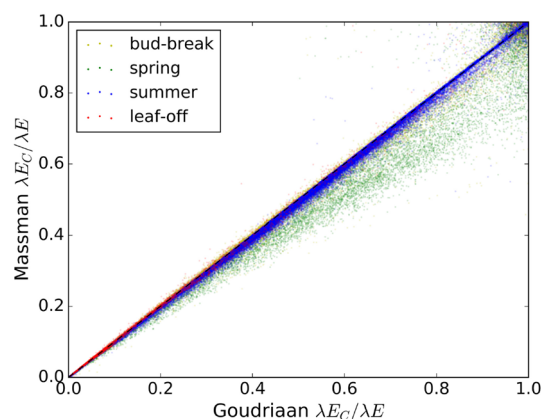
2016; Zúñiga et al. 2018). This approach assumes that the water consumed for a given crop and phenological stage is linearly related to a grass or alfalfa reference evapotranspiration (e.g., Allen et al. 1998 FAO-56 or Walter et al. 2000 ASCE). However, the radiative and aerodynamic regime in a heterogeneous row crop is likely to deviate from these simple empirical relationships. Indeed this refined model, which also includes the effect of hedgerow structure in energy partitioning (Parry et al. 2018) as well as aerodynamic roughness variations with wind direction (Alfieri et al. 2018a), can be incorporated into a two-source energy combination model (Shuttleworth and Wallace 1985; Brenner and Incoll 1997) and estimate water use and energy use efficiency separately for the row crop and interrow. This would result in more a robust definition of crop water needs for future irrigation experiments. Moreover, this modelling framework could be further developed using a canopy conductance model to run simulations using different vineyard trellis configurations, vine varieties and management scenarios that would provide optimal solutions for designing row spacing and trellis systems when planting new vineyards in different climate regions.

On the other hand, regulated deficit irrigation (RDI) is a regular strategy in viticulture to submit a moderate stress to the vines thus increasing yield quality. Crop stress has been usually defined from measurements of water potential $\Psi$ (either leaf, stem or pre-dawn, Flexas et al. 2004) and hence several studies have proposed $\Psi$ thresholds when applying RDI (van Leeuwen et al. 2009; Girona et al. 2006; Intrigliolo et al. 2016; Merli et al. 2016). Nevertheless, these $\Psi$ thresholds may vary depending on root distribution, vine vigour, yield, and/or isohydric/anisohydric varieties (van Leeuwen et al. 2009; Romero et al. 2010; Flexas et al. 2004). Therefore, other authors suggested that stomatal conductance $g_s$ is a more precise and sensitive indicator of water stress than $\Psi$ (Romero et al. 2010; Cifre et al. 2005). Measurements of

$g_s$ (Zúñiga et al. 2018; Romero et al. 2010; Cifre et al. 2005; Flexas et al. 2004) or sap-flow measurements (Eastham and Gray 1998; Ginestar et al. 1998; Patakas et al. 2005) have therefore been conducted as proxy for canopy transpiration and assimilation in RDI. With a correct ET partitioning in TSEB, robust and spatially distributed estimates of canopy transpiration can be obtained either from in situ (Kustas et al. 2018b), airborne (Nieto et al. 2018) or satellite (Knipper et al. 2018) data, from which it is possible to derive effective values of stomatal conductance from top–down approaches (Baldocchi et al. 1991), similar to the ones proposed in Jones et al. (2002), Leinonen et al. (2006), or Berni et al. (2009). This type of approach using Earth observations has a major advantage from traditional techniques used in vineyard water management in that it has the capability of mapping in a spatially distributed manner water use and stress conditions over large areas.

# Conclusions

This study evaluated a new wind attenuation profile that explicitly considers the vertical heterogeneity in foliage distribution in canopies such as row crops. In a first stage, our results indicated that the Massman et al. (2017) profile did not improve the modelled wind speed in the interrow below the canopy in two, respectively, mature and young vineyards. However, when the new proposed wind profile was implemented in the Two Source Energy Balance model (Kustas and Norman 1999; Kustas et al. 2016), an improvement in the estimation of sensible heat flux was found during spring, when there coexist two vegetative layers, an upper horizontally discontinuous canopy with heterogeneous vertical distribution of foliage, and a lower more homogeneous grass layer of little height.

Similar to the findings of Cammalleri et al. (2010), wind profile attenuation modelling has been shown to have an effect on clumped canopies with moderate vegetation density. Before bud-break and after grapevine leaf-off, the canopy extinction effect is fairly small, while during summer, as the canopy in our study sites become well developed with a lower vertical and horizontal discontinuity, the new Massman et al. (2017) attenuation profile resembles more to the Goudriaan (1977) profile. The younger vineyard in the South gave a better performance with Massman et al. (2017) as its canopy is less developed, more clumped and with a larger influence of the cover crop layer in the interrow. Nevertheless, in future research additional sites will be evaluated under the hypothesis that Massman et al. (2017) profile has a larger potential use in more clumped canopies with more significant vertically non-uniform biomass distributions such as Vertical Shoot Position VSP vineyards,

tree wall (i.e., central leader system) orchards, as well as in wooded savannah.

Although the impact on irrigation and possible savings in water is not the focus or topic of this study—as this will depend on irrigation strategies (full irrigation, controlled deficit irrigation, support irrigation), as well as the available technology for irrigation and its efficiency—we believe that the improvement of irrigation systems will require integrating these types of energy balance models that can create evapotranspiration and transpiration maps with soil water balance models. This topic requires, therefore, a separate study and paper. In addition, more reliable ET partitioning using two-source energy balance models with the proposed wind attenuation profile will be necessary to account more accurately, crop water use and requirements.

# Appendix: TSEB model

The basic equation of the energy balance at the surface can be expressed following Eq. 4.

$$R_n \approx H + \lambda E + G \tag{4a}$$

$$R_{n,S} \approx H_S + \lambda E_S + G \tag{4b}$$

$$R_{n,C} \approx H_C + \lambda E_C \tag{4c}$$

with $R_n$ being the net radiation, $H$ the sensible heat flux, $\lambda E$ the latent heat flux or evapotranspiration, and $G$ the soil heat flux. "C" and "S" subscripts refer to canopy and soil layers, respectively. The symbol "$\approx$" appears since there are additional components of the energy balance that are usually neglected, such as heat advection, storage of energy in the canopy layer or energy for the fixation of $CO_2$ (Hillel 1998).

The key in TSEB models is the partition of sensible heat flux into the canopy and soil layers, which depends on the soil and canopy temperatures ($T_S$ and $T_C$, respectively). If we assume that there is an interaction between the fluxes of canopy and soil, due to an expected heating of the in-canopy air by heat transport coming from the soil, the resistances network in TSEB can be considered to be in series. In that case $H$ can be estimated as in Eq. 5 (Norman et al. 1995, Eqs. A1–A3)

$$H = H_C + H_S = \rho_{air} C_p \frac{T_{AC} - T_A}{R_a}$$
$$= \rho_{air} C_p \left[ \frac{T_C - T_{AC}}{R_x} + \frac{T_S - T_{AC}}{R_s} \right] \quad (5)$$

where $\rho_{air}$ is the density of air (kg m$^{-3}$), $C_p$ is the heat capacity of air at constant pressure (J kg$^{-1}$ K$^{-1}$), $T_{AC}$ is the air temperature at the canopy interface, equivalent to the aerodynamic temperature $T_0$, computed with Eq. 6 (Norman et al. 1995, Eq. 4).

$$T_{AC} = \frac{\frac{T_A}{R_a} + \frac{T_C}{R_x} + \frac{T_S}{R_s}}{\frac{1}{R_a} + \frac{1}{R_x} + \frac{1}{R_s}}. \quad (6)$$

Here $R_a$ is the aerodynamic resistance to heat transport (s m$^{-1}$), $R_s$ is the resistance to heat flow in the boundary layer immediately above the soil surface (s m$^{-1}$), and $R_x$ is the boundary layer resistance of the canopy of leaves (s m$^{-1}$). The mathematical expressions of these resistances are detailed in Eq. 7 and in Norman et al. (1995) and Kustas and Norman (2000) and discussed in Kustas et al. (2016).

$$R_a = \frac{\ln\left(\frac{z_T - d_0}{z_{0H}}\right) - \Psi_h\left(\frac{z_T - d_0}{L}\right) + \Psi_h\left(\frac{z_{0H}}{L}\right)}{\kappa' u_*} \quad (7a)$$

$$R_s = \frac{1}{c\left(T_S - T_A\right)^{1/3} + b\, u_s} \quad (7b)$$

$$R_x = \frac{C'}{LAI} \left( \frac{l_w}{U_{d_0 + z_{0M}}} \right)^{1/2} \quad (7c)$$

where $u_*$ is the friction velocity (m s$^{-1}$) computed as:

$$u_* = \frac{\kappa' u}{\left[ \ln\left(\frac{z_u - d_0}{z_{0M}}\right) - \Psi_m\left(\frac{z_u - d_0}{L}\right) + \Psi_m\left(\frac{z_{0M}}{L}\right) \right]}. \quad (8)$$

In Eq. 8 $z_u$ and $z_T$ are the measurement heights for wind speed $u$ (m s$^{-1}$) and air temperature $T_A$ (K), respectively. $d_0$ is the zero-plane displacement height, $z_{0M}$ and $z_{0H}$ are the roughness length for momentum and heat transport, respectively (all those magnitudes expressed in m), with $z_{0H} = z_{0M} \exp(-kB^{-1})$. In the series version of TSEB $z_{0H}$ is assumed equal to $z_{0M}$ since the term $R_x$ already accounts for the different efficiency between heat and momentum transport (Norman et al. 1995), and therefore $kB^{-1} = 0$. The value of $\kappa' = 0.4$ is the von Karman's constant. The $\Psi_m(\zeta)$ terms in Eqs. 7a and 8 are the adiabatic correction factors for momentum. The formulations of these two factors

are described in Brutsaert (1999, 2005). These corrections depend on the atmospheric stability, which is expressed using the Monin–Obukhov length $L$ (m):

$$L = \frac{-u_*^3 \rho_{air}}{kg\left[ \frac{H}{(T_A C_p)} + 0.61E \right]} \quad (9)$$

where $H$ is the bulk sensible heat flux (W m$^{-2}$), $E$ is the rate of surface evaporation (kg s$^{-1}$), and $g$ the acceleration of gravity (m s$^{-2}$).

The coefficients $b$ and $c$ in Eq. 7b depend on turbulent length scale in the canopy, soil-surface roughness and turbulence intensity in the canopy, which are discussed in Sauer et al. (1995), Kondo and Ishida (1997) and Kustas et al. (2016). $C'$ is assumed to be 90 s$^{1/2}$ m$^{-1}$ and $l_w$ is the average leaf width (m).

Wind speed at the heat source–sink ($z_{0M} + d_0$) and near the soil surface was originally estimated using Goudriaan (1977) wind attenuation model (Eq. 10)

$$U(z) = U_C \exp\left[ -a_G\left(1 - z/h_c\right) \right] \quad (10)$$

$$a_G = 0.28 LAI^{2/3} h_c^{1/3} l_w^{-1/3}. \quad (11)$$

Since Eqs. 5–9 are interrelated, an iterative scheme is performed until the convergence of $L$ and $u_*$ is reached. The iterative process is as follows: neutral conditions are firstly assumed ($L \to \infty$, $\Psi_M(\zeta) = 0$ and $\Psi_H(\zeta) = 0$) and an initial estimate of $H$ is calculated using Eqs. 8 to 5, and $E$ with Eq. 4. An initial value of $L$ is then obtained from Eq. 9 and the stability functions are then calculated, which gives a new friction velocity (Eq. 8) and resistance set (Eq. 7) and new estimates of $H$ and $E$ (Eqs. 6, 5 and 4). $L$ is recalculated again and the process continues (Eqs. 9–5) until the change in $L$ and $u_*$ between two successive iterations is lower than a certain threshold.

When only a single observation of $T_{rad}$ is available (i.e., measurement at a single angle), partitioning of $T_{rad}$ requires some assumptions to help to define $T_C$ or $T_S$. One approach developed for TSEB (Norman et al. 1995) starts with an initial estimate that assumes plants are transpiring at a potential rate, as defined by the Priestley and Taylor (1972) relationship, applied to the canopy divergence of net radiation ($R_{n,C}$)

$$\lambda E_C = \alpha_{PT} f_g \frac{\Delta}{\Delta + \gamma} R_{n,C} \quad (12)$$

where $\alpha_{PT}$ is the Priestley–Taylor coefficient, initially set to 1.26, $f_g$ is the fraction of vegetation that is green and hence capable of transpiring, $\Delta$ is the slope of the saturation vapor pressure versus temperature curve, and $\gamma$ is the psychrometric constant. This allows the canopy-sensible heat flux to be calculated using the energy-balance at the canopy layer ($H_c = R_{n,C} - \lambda E_C$) and hence an estimate of $T_C$ to be

obtained by inverting Eq. 5 (Norman et al. 1995, Eqs. A7, A11 and A12). Then $T_S$ is the derived from Eq. 13 having both $T_{rad}$ and $T_C$ and an estimate of $f_c(\theta)$ the fraction of vegetation observed by the sensor view zenith angle $\theta$.

$$T_{rad}^4(\theta) = f_c(\theta)T_C^4 + \left[1 - f_c(\theta)\right]T_S^4. \tag{13}$$

The value of $f_c(\theta)$ is typically estimated as an exponential function of the leaf area index, which includes a clumping factor or index $\Omega$ for row crops and canopies where the LAI is concentrated for plants sparsely distributed or are organized such as row crops (Kustas and Norman 1999; Anderson et al. 2005) and has the following form.

$$f_c(\theta) = 1 - \exp\left(\frac{-0.5\Omega LAI}{\cos\theta}\right). \tag{14}$$

If the initial $T_C$ implied by this approximation is unusually low in comparison with the observed $T_{rad}$, $T_S$ will likely be overestimated and therefore produce unrealistic estimates of soil latent heat flux (negative values during daytime). In this case, the $\alpha_{PT}$ coefficient is iteratively reduced assuming the canopy is stressed and transpiring at sub-potential levels until soil latent heat flux becomes zero or positive.

# References

Alfieri J, Kustas W, Gao F, Prueger J, Nieto H, Hipps L (2018a) Influence of wind direction on the effective surface roughness of vineyards. Irrig Sci (this issue)

Alfieri JG, Kustas WP, Prueger JH, McKee LG, Hipps LE, Gao F (2018b) A multi-year intercomparison of micrometeorological observations at adjacent vineyards in California's Central Valley during GRAPEX. Irrig Sci. https://doi.org/10.1007/s00271-018-0599-3

Allen RG, Pereira LS, Raes D, Smith M (1998) Crop evapotranspiration—guidelines for computing crop water requirements-FAO irrigation and drainage paper 56, vol 300(9). FAO, Rome, p D05109

Anderson MC, Norman JM, Kustas WP, Li F, Prueger JH, Mecikalski JR (2005) Effects of vegetation clumping on two-source model estimates of surface energy fluxes from an agricultural landscape during SMACEX. J Hydrometeorol 6(6):892–909

Baldocchi DD, Luxmoore RJ, Hatfield JL (1991) Discerning the forest from the trees: an essay on scaling canopy stomatal conductance. Agric For Meteorol 54(2):197–226. https://doi.org/10.1016/0168-1923(91)90006-C

Bastiaanssen W, Pelgrum H, Wang J, Ma Y, Moreno J, Roerink G, van der Wal T (1998) A remote sensing surface energy balance algorithm for land (SEBAL): part 2: validation. J Hydrol 212–213:213–229

Bellvert J, Zarco-Tejada P, Marsal J, Girona J, González-Dugo V, Fereres E (2016) Vineyard irrigation scheduling based on airborne thermal imagery and water potential thresholds. Aust J Grape Wine Res 22(2):307–315

Berni J, Zarco-Tejada P, Sepulcre-Cantó G, Fereres E, Villalobos F (2009) Mapping canopy conductance and CWSI in olive orchards using high resolution thermal remote sensing imagery. Remote Sens Environ 113(11):2380–2388

Brenner A, Incoll L (1997) The effect of clumping and stomatal response on evaporation from sparsely vegetated shrublands. Agric For Meteorol 84(3):187–205

Brutsaert W (1999) Aspects of bulk atmospheric boundary layer similarity under free-convective conditions. Rev Geophys 37(4):439–451

Brutsaert W (2005) Hydrology. An introduction. Cambridge University Press, Cambridge

Cammalleri C, Anderson MC, Ciraolo G, D'Urso G, Kustas WP, La Loggia G, Minacapilli M (2010) The impact of in-canopy wind profile formulations on heat flux estimation in an open orchard using the remote sensing-based two-source model. Hydrol Earth Syst Sci 14(12):2643–2659

Campbell GS, Norman JM (1998) An introduction to environmental biophysics, 2nd edn. Springer, New York

Choudhury B, Idso S, Reginato R (1987) Analysis of an empirical model for soil heat flux under a growing wheat crop for estimating evaporation by an infrared-temperature based energy balance equation. Agric For Meteorol 39(4):283–297

Cifre J, Bota J, Escalona J, Medrano H, Flexas J (2005) Physiological tools for irrigation scheduling in grapevine (*Vitis vinifera* L.): an open gate to improve water-use efficiency? Agric Ecosyst Environ 106(2):159–170. https://doi.org/10.1016/j.agee.2004.10.005

Colaizzi P, Evett S, Howell T, Li F, Kustas W, Anderson M (2012) Radiation model for row crops: I. Geometric view factors and parameter optimization. Agron J 104(2):225–240

Eastham J, Gray SA (1998) A preliminary evaluation of the suitability of sap flow sensors for use in scheduling vineyard irrigation. Am J Enol Vitic 49(2):171–176

Flexas J, Bota J, Cifre J, Mariano Escalona J, Galmés J, Gulías J, Lefi EK, Florinda Martínex-Cañellas S, Teresa Moreno M, Ribas-Carbó M, Riera D, Samplo B, Medrano H (2004) Understanding down-regulation of photosynthesis under water stress: future prospects and searching for physiological tools for irrigation management. Ann Appl Biol 144(3):273–283. https://doi.org/10.1111/j.1744-7348.2004.tb00343.x

Foken T (2008) The energy balance closure problem: an overview. Ecol Appl 18(6):1351–1367

Gao F, Kustas WP, Anderson MC (2012) A data mining approach for sharpening thermal satellite imagery over land. Remote Sens 4(11):3287

Gao F, Anderson M, Kustas W, Houborg R (2014) Retrieving leaf area index from Landsat using MODIS LAI products and field measurements. IEEE Geosci Remote Sens Lett 11(4):773–777

Ginestar C, Eastham J, Gray S, Iland P (1998) Use of sap-flow sensors to schedule vineyard irrigation. I. Effects of post-veraison water deficits on water relations, vine growth, and yield of Shiraz grapevines. Am J Enol Vitic 49(4):413–420

Girona M, Mata J, del Campo J, Arbonés A, Bartra E, Marsal J (2006) The use of midday leaf water potential for scheduling deficit irrigation in vineyards. Irrig Sci 24(2):115–127. https://doi.org/10.1007/s00271-005-0015-7

Goring DG, Nikora VI (2002) Despiking acoustic doppler velocimeter data. J Hydraul Eng 128(1):117–126

Goudriaan J (1977) Crop micrometeorology: a simulation stud. Technical report, Center for Agricultural Publications and Documentation, Wageningen

Heilman J, McInnes K, Savage M, Gesch R, Lascano R (1994) Soil and canopy energy balances in a west Texas vineyard. Agric For Meteorol 71(1):99–114

Hillel D (1998) Environmental soil physics. Academic Press, Cambridge

Intrigliolo D, Lizama V, García-Esparza M, Abrisqueta I, Álvarez I (2016) Effects of post-veraison irrigation regime on Cabernet Sauvignon grapevines in valencia, Spain: yield and grape composition. Agric Water Manag 170:110–119. https://doi.org/10.1016/j.agwat.2015.10.020 Special Issue: Water Management Strategies in Irrigated Areas Overseen by: Dr. Brent Clothier

Jones HG, Stoll M, Santos T, Sousa Cd, Chaves MM, Grant OM (2002) Use of infrared thermography for monitoring stomatal closure in the field: application to grapevine. J Exp Bot 53(378):2249–2260. https://doi.org/10.1093/jxb/erf083

Kalma JD, McVicar TR, McCabe MF (2008) Estimating land surface evaporation: a review of methods using remotely sensed surface temperature data. Surv Geophys 29(4):421–469

Knipper KR, Kustas WP, Anderson MC, Alfieri JG, Prueger JH, Hain CR, Gao F, Yang Y, McKee LG, Nieto H, Hipps LE, Alsina MM, Sánchez L (2018) Evapotranspiration estimates derived using thermal-based satellite remote sensing and data fusion for irrigation management in California vineyards. Irrig Sci. https://doi.org/10.1007/s00271-018-0591-y

Kondo J, Ishida S (1997) Sensible heat flux from the earth's surface under natural convective conditions. J Atmos Sci 54(4):498–509

Kool D, Agam N, Lazarovitch N, Heitman J, Sauer T, Ben-Gal A (2014) A review of approaches for evapotranspiration partitioning. Agric For Meteorol 184:56–70

Kustas W, Anderson M (2009) Advances in thermal infrared remote sensing for land surface modeling. Agric For Meteorol 149(12):2071–2081 Environmental Biophysics—Tribute to John Norman

Kustas WP, Norman JM (1999) Evaluation of soil and vegetation heat flux predictions using a simple two-source model with radiometric temperatures for partial canopy cover. Agric For Meteorol 94(1):13–29

Kustas W, Norman J (2000) A two-source energy balance approach using directional radiometric temperature observations for sparse canopy covered surfaces. Agron J 92(5):847–854

Kustas WP, Nieto H, Morillas L, Anderson MC, Alfieri JG, Hipps LE, Villagarcía L, Domingo F, García M (2016) Revisiting the paper "Using radiometric surface temperature for surface energy flux estimation in Mediterranean drylands from a two-source perspective". Remote Sens Environ 184:645–653

Kustas W, Alfieri J, Nieto H, Wilson T, Gao F, Anderson M (2018a) Utility of the two-source energy balance model TSEB in vine and inter-row flux partitioning over the growing season. Irrig Sci. https://doi.org/10.1007/s00271-018-0586-8

Kustas WP, Anderson MC, Alfieri JG, Knipper K, Torres-Rua A, Parry CK, Nieto H, Agam N, White WA, Gao F, McKee L, Prueger JH, Hipps LE, Los S, Alsina MM, Sanchez L, Sams B, Dokoozlian N, McKee M, Jones S, Yang Y, Wilson TG, Lei F, McElrone A, Heitman JL, Howard AM, Post K, Melton F, Hain C (2018b) The grape remote sensing atmospheric profile and evapotranspiration experiment. Bull Am Meteorol Soc 99(9):1791–1812. https://doi.org/10.1175/BAMS-D-16-0244.1

Lalic B, Mihailovic D, Rajkovic B, Arsenic I, Radlovic D (2003) Wind profile within the forest canopy and in the transition layer above it. Environ Model Softw 18(10):943–950

Leinonen I, Grat OM, Tagliavia CPP, Chaves MM, Jones HG (2006) Estimating stomatal conductance with thermal imagery. Plant Cell Environ 29(8):1508–1518. https://doi.org/10.1111/j.1365-3040.2006.01528.x

Massman W (1987) A comparative study of some mathematical models of the mean wind structure and aerodynamic drag of plant canopies. Bound Layer Meteorol 40(1):179–197

Massman W (2000) A simple method for estimating frequency response corrections for eddy covariance systems. Agric For Meteorol 104(3):185–198

Massman W, Forthofer J, Finney M (2017) An improved canopy wind model for predicting wind adjustment factors and wildland fire behavior. Can J For Res 47(5):594–603

McInnes K, Heilman J, Lascano R (1996) Aerodynamic conductances at the soil surface in a vineyard. Agric For Meteorol 79(1):29–37

McNaughton K, Van Den Hurk B (1995) A "Lagrangian" revision of the resistors in the two-layer model for calculating the energy budget of a plant canopy. Bound Layer Meteorol 74(3):261–288

Merli M, Magnanini E, Gatti M, Pirez F, Pueyo IB, Intrigliolo D, Poni S (2016) Water stress improves whole-canopy water use efficiency and berry composition of cv. Sangiovese (*Vitis vinifera* L.) grapevines grafted on the new drought-tolerant rootstock m4. Agric Water Manag 169:106–114. https://doi.org/10.1016/j.agwat.2016.02.025

Nieto H, Kustas WP, Torres-Rúa A, Alfieri JG, Gao F, Anderson MC, White WA, Song L, del Mar Alsina M, Prueger JH, McKee M, Elarab M, McKee LG (2018) Evaluation of TSEB turbulent fluxes using different methods for the retrieval of soil and canopy component temperatures from UAV thermal and multispectral imagery. Irrig Sci. https://doi.org/10.1007/s00271-018-0585-9

Norman JM, Kustas WP, Humes KS (1995) Source approach for estimating soil and vegetation energy fluxes in observations of directional radiometric surface temperature. Agric For Meteorol 77(3–4):263–293

Oke TR, Cleugh HA (1987) Urban heat storage derived as energy balance residuals. Bound Layer Meteorol 39(3):233–245

Ortega-Farias S, Carrasco M, Olioso A, Acevedo C, Poblete C (2007) Latent heat flux over Cabernet Sauvignon vineyard using the Shuttleworth and Wallace model. Irrig Sci 25(2):161–170

Parry C, Nieto H, Guillevic P, Agam N, Kustas B, Alfieri J, McKee L, McElrone A (2018) An intercomparison of radiation partitioning models in vineyard row structured canopies. Irrig Sci (this issue)

Patakas A, Noitsakis B, Chouzouri A (2005) Optimization of irrigation water use in grapevines using the relationship between transpiration and plant water status. Agric Ecosyst Environ 106(2):253–259. https://doi.org/10.1016/j.agee.2004.10.013

Priestley CHB, Taylor RJ (1972) On the assessment of surface heat flux and evaporation using large-scale parameters. Mon Weather Rev 100(2):81–92

Raupach MR (1994) Simplified expressions for vegetation roughness length and zero-plane displacement as functions of canopy height and area index. Bound Layer Meteorol 71(1):211–216

Romero P, Fernández-Fernández JI, Martínez-Cutillas A (2010) Physiological thresholds for efficient regulated deficit-irrigation management in winegrapes grown under semiarid conditions. Am J Enol Vitic 61(3):300–312

Romero P, Pérez-Pérez JG, del Amor FM, Martinez-Cutillas A, Dodd IC, Botía P (2014) Partial root zone drying exerts different physiological responses on field-grown grapevine (*Vitis vinifera* cv. Monastrell) in comparison to regulated deficit irrigation. Funct Plant Biol 41(11):1087–1106

Santanello J Jr, Friedl M (2003) Diurnal covariation in soil heat flux and net radiation. J Appl Meteorol 42(6):851–862

Sauer TJ, Norman JM, Tanner CB, Wilson TB (1995) Measurement of heat and vapor transfer coefficients at the soil surface beneath a maize canopy using source plates. Agric For Meteorol 75(1–3):161–189

Scanlon TM, Kustas WP (2010) Partitioning carbon dioxide and water vapor fluxes using correlation analysis. Agric For Meteorol 150(1):89–99

Scanlon TM, Kustas WP (2012) Partitioning evapotranspiration using an eddy covariance-based technique: improved assessment of soil moisture and land–atmosphere exchange dynamics. Vadose Zone J 11(3):vzj2012.0025. https://doi.org/10.2136/vzj2012.0025

Scanlon TM, Sahu P (2008) On the correlation structure of water vapor and carbon dioxide in the atmospheric surface layer: a basis for flux partitioning. Water Resour Res 44(10):W10418. https://doi.org/10.1029/2008WR006932

Shuttleworth WJ, Gurney RJ (1990) The theoretical relationship between foliage temperature and canopy resistance in sparse crops. Q J R Meteorol Soc 116(492):497–519

Shuttleworth WJ, Wallace JS (1985) Evaporation from sparse crops—an energy combination theory. Q J R Meteorol Soc 111(469):839–855

Sobrino JA, Jiménez-Muñoz JC, Verhoef W (2005) Canopy directional emissivity: comparison between models. Remote Sens Environ 99(3):304–314

Sun L, Gao F, Anderson MC, Kustas WP, Alsina MM, Sanchez L, Sams B, McKee L, Dulaney W, White WA, Alfieri JG, Prueger JH, Melton F, Post K (2017) Daily mapping of 30 m LAI and NDVI for grape yield prediction in California vineyards. Remote Sens 9(4):317

Tanner CB, Thurtell GW (1969) Anemoclinometer measurements of Reynolds stress and heat transport in the atmospheric surface layer. Technical report, Wisconsin University-Madison, Department of Soil Science

Teixeira AHC, Bastiaanssen WGM, Bassoi LH (2007) Crop water parameters of irrigated wine and table grapes to support water productivity analysis in the São Francisco river basin. Brazil. Agric Water Manag 94(1):31–42

van der Kwast J, Timmermans W, Gieske A, Su Z, Olioso A, Jia L, Elbers J, Karssenberg D, de Jong S (2009) Evaluation of the surface energy balance system (SEBS) applied to ASTER imagery with flux-measurements at the SPARC 2004 site (Barrax, Spain). Hydrol Earth Syst Sci 13(7):1337–1347

van Leeuwen C, Trégoat O, Choné X, Bois B, Pernet D, Gaudillère JP (2009) Vine water status is a key factor in grape ripening and vintage quality for red bordeaux wine. How can it be assessed for vineyard management purposes? OENO One 43(3):121–134. https://doi.org/10.20870/oeno-one.2009.43.3.798

Walter IA, Allen RG, Elliott R, Jensen ME, Itenfisu D, Mecham B, Howell TA, Snyder R, Brown P, Echings S, Spofford T, Hattendorf M, Cuenca RH, Wright JL, Martin D (2000) ASCE's standardized reference evapotranspiration equation. In: Watershed Management and Operations Management 2000. https://doi.org/10.1061/40499(2000)126

Webb EK, Pearman GI, Leuning R (1980) Correction of flux measurements for density effects due to heat and water vapour transfer. Q J R Meteorol Soc 106(447):85–100

Willmott CJ (1981) On the validation of models. Phys Geogr 2(2):184–194

Zhang B, Kang S, Li F, Zhang L (2008) Comparison of three evapotranspiration models to Bowen ratio-energy balance method for a vineyard in an arid desert region of northwest China. Agric For Meteorol 148(10):1629–1640

Zipper SC, Loheide SP II (2014) Using evapotranspiration to assess drought sensitivity on a subfield scale with HRMET, a high resolution surface energy balance model. Agric For Meteorol 197:91–102

Zúñiga M, Ortega-Farías S, Fuentes S, Riveros-Burgos C, Poblete-Echeverría C (2018) Effects of three irrigation strategies on gas exchange relationships, plant water status, yield components and water productivity on grafted Carménère grapevines. Front Plant Sci. https://doi.org/10.3389/fpls.2018.00992